DBD plasma-assisted ethanol steam reforming for green H_2 production: process optimization through response surface methodology (RSM)

Guoqiang Cao,[1] Yue Xiao,[2] Wei-Min Huang,[3] Chien-Hua Chen[2] and Jonas Baltrusaitis[1,*]

[1]Department of Chemical and Biomolecular Engineering, Lehigh University, B336 Iacocca Hall, 111 Research Drive, Bethlehem, Pennsylvania 18015, United States

[2]Advanced Cooling Technologies, Inc., 1046 New Holland Avenue, Lancaster, Pennsylvania 17601, United States

[3]Department of Mathematics, Lehigh University, Christmas-Saucon Hall, E Packer Ave, Bethlehem, Pennsylvania 18015, United States

Abstract

This work investigates ethanol steam reforming (ESR) to produce hydrogen (H_2) in a dielectric barrier discharge (DBD) plasma reactor. A five-level, three-factor experiment design was performed using a response surface methodology (RSM) to evaluate the combined effects of the three process parameters, including discharge power, total flow rate, and ethanol-to-water ($EtOH/H_2O$) molar ratio on the plasma-assisted ESR reaction. Quadratic regression models were employed in RSM to fit the experimental results and present the correlation between process parameters and targeted responses (EtOH conversion, H_2 yield, H_2 selectivity, and specific energy requirement (SER) for H_2 production). The results suggested that the $EtOH/H_2O$ molar ratio is considered to have the most significant effect on the EtOH conversion and H_2, H_2 selectivity, while the total flow rate is the most significant parameter determining SER for H_2 production. Process optimization demonstrated the optimal process conditions, including a discharge power of 55.9 W, a total flow rate of 26.7 ml/min, and an $EtOH/H_2O$ molar ratio equal to 0.34. A validation test was performed and confirmed the feasibility of the optimization process.

Keywords:

Ethanol steam reforming; Green hydrogen; Dielectric barrier discharge; Response surface methodology; Process optimization

Corresponding author: job314@lehigh.edu. +1-610-758-6838

1. Introduction

Sustained world population growth, industrial development, and urbanization resulted in an increased demand for energy. The majority of energy is generated using non-renewable fossil fuels, which lead to greenhouse gas emissions and global warming. The use of finite fossil fuel reserves needs to be addressed using sustainable energy sources [1]. In one of the scenarios to increase energy sustainability, hydrogen (H_2) has been proposed as a promising energy carrier to minimize the dependence on fossil fuels and reduce environmental concerns [2–4]. Hydrogen can be derived from renewable feedstock, which can result in zero greenhouse gas emissions. Additionally, the energy content per unit mass of hydrogen is three times higher than that of gasoline [5]. Various technologies have already been developed to produce hydrogen from fossil fuels as well as renewable feedstock, including water electrolysis, catalytic partial oxidation, autothermal reforming of hydrocarbons and coal, steam reforming, and biomass gasification [6–12]. An encouraging development in light of its sustainable generation is the steam reforming of hydrocarbons and oxygenates produced from biomass, such as ethanol (EtOH) [13,14].

Ethanol steam reforming (ESR) possesses the following advantages when compared with the other hydrogen production methods: high hydrogen content in ethanol molecule, its high energy density, renewability, and easy storage, while also taking place at lower operating temperatures than partial oxidation or autothermal reforming [2,15–19]. ESR is a complex process that can be described via the primary reaction, as expressed in Eq. (1), where CO_2 produced can be taken up to yield more biomass

$$C_2H_5OH + 3H_2O \rightarrow 6H_2 + 2CO_2 \qquad \Delta H = 173 \text{ kJ/mol} \qquad (1)$$

The actual reaction includes several pathways determined by operating conditions and catalysts. A wide range of catalysts on various supports has been developed for conventional (catalytic) ESR reactions, while the overall catalytic performance is dramatically affected by the reaction temperature. The reaction temperature of at least ~700 ^{o}C is typically used to achieve near-equilibrium conversion for a high hydrogen yield, while lower temperatures result in side reactions and by-product generation [3]. To achieve such temperatures, an external fuel source is still needed, which generates CO_2 emissions, thus reducing the overall sustainability of the process.

Non-thermal plasma has shown advancements and promises in enhanced sustainability for fuel reforming technology and ammonia synthesis due to its high energy density, low-temperature operation conditions, rapid start-up time, and low energy cost [20–26]. The non-thermal plasma reactors have been designed based on the various plasma sources, such as gliding arc discharge (GAD) [23,27–29], microwave discharge (MWD) [30–34], dielectric barrier discharge (DBD) [35–38], and glow discharge [39–41]. This technique has also been proposed to provide energy for the ESR reaction, as determined by a range of process parameters, such as power, feed flow rate, and feed composition. In particular, previous studies on plasma-assisted ethanol reforming had focused on the effect of a single parameter on the catalytic performance [42,43], while the interactive influence of different parameters was lacking in the investigation. Response surface methodology (RSM), a statistical technique, is commonly used to provide the optimal process parameters based on the design of experiments [44–46]. RSM can evaluate the individual process variables, develop optimization models, and determine the interaction between each parameter as visualized by 3D response surface and contour plots. So far, the RSM has been chiefly applied to optimize different plasma catalytic reactions, such as dry methane reforming [47,48] and toluene degradation [49], ammonia synthesis [50], while using RSM to investigate the DBD plasma-assisted ESR has not been attempted.

In this study, we investigated ethanol steam reforming in a DBD plasma reactor. As a first step, a homogeneous, non-catalytic process was considered. The effect of process variables, including the discharge power, total flow rate, and ethanol to steam molar ratio, were analyzed using the RSM. The interactive effects of each parameter on the reaction performance were discussed, and optimal conditions were proposed and further validated.

2. Experimental

2.1 Experimental setup

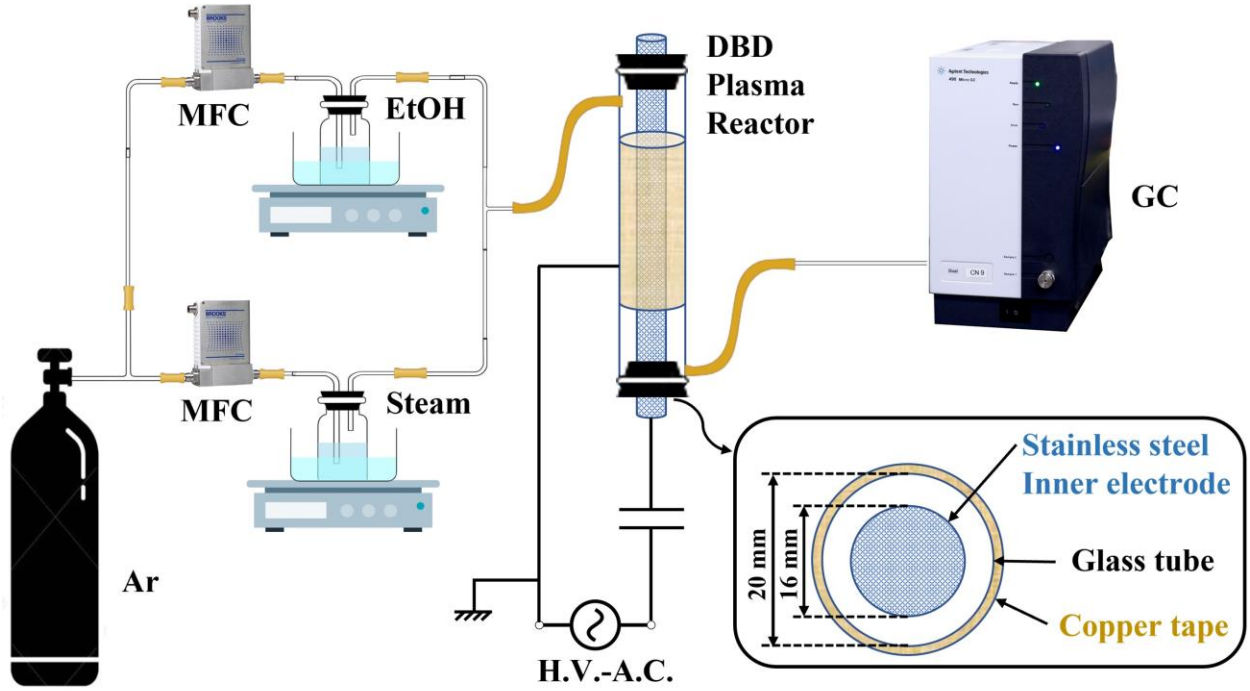

Figure 1 Schematic diagram of the experimental setup.

The experimental setup of EtOH steam reforming in a DBD non-thermal plasma reactor is shown in Figure 1 and was comprised of an EtOH vapor and steam generation system, a DBD plasma reactor, an AC high voltage power supply, and gaseous product analysis. The reactor was a stainless-steel inner electrode with an outer diameter of 16 mm and a glass tube with an internal diameter of 20 mm, which was covered with copper tape as the outer electrode. The length of the copper tape was 140 mm. The experimental setup was adopted from the previous work [22,51,52]. Argon was used as the carrier gas and its flow rate was controlled by mass flow rate controllers, while EtOH and H_2O flow rates were calculated using Eq. (2)

$$\frac{Q_{Ar}}{Q_{EtOH\ or\ H_2O}} = \frac{101.325\ kPa - P_{EtOH\ or\ H_2O}}{P_{EtOH\ or\ H_2O}} \quad (2)$$

where Q is the flow rate of Ar, EtOH, and H_2O and $P_{EtOH\ or\ H_2O}$ is the saturated partial pressure of EtOH or H_2O at a selected temperature. In a typical test, EtOH vapor and steam generators were first preheated to selected temperature, argon gas (60 ml/min) was then flown through the EtOH

and steam generator to generate saturated vapor containing stream. The mixture of the vapors was introduced to the DBD plasma reactor. After the steady state flow of the reactant vapors was achieved, plasma with certain discharge power was applied. The gas products were analyzed using micro gas chromatography (GC, Agilent 490 Micro), which was equipped with a flame ionization detector and a thermal conductivity detector. It contained 2-channels equipped with a MolSieve 5A (MS5A) and PLOT Q columns. The MS5A column was used to separate H_2, CO, and CH_4, while the PLOT Q column was used to identify CO_2. This allowed quantitative analysis of the data. EtOH conversion, H_2 yield, H_2 selectivity, and specific energy requirement (SER) for H_2 production were evaluated using (3) through (6) [53,54].

The ethanol conversion rate:

$$C_{EtOH}(\%) = \frac{n_{CO}+n_{CH_4}+n_{CO_2}}{2n_{EtOH\ input}} \times 100 \quad (3)$$

The yield (Y) of H_2:

$$Y_{H_2}(\%) = \frac{n_{H_2\ produced}}{3n_{EtOH\ input}} \times 100 \quad (4)$$

The selectivity (S) of H_2:

$$S_{H_2}(\%) = \frac{n_{H_2\ produced}}{3n_{EtOH\ input} \times C_{EtOH}} \times 100 \quad (5)$$

SER for H_2 production:

$$SER_{H_2}(kJ/mol) = \frac{Discharge\ power}{n_{H_2\ produced}} \quad (6)$$

2.2 Experimental design and response surface methodology (RSM)

Response surface methodology was employed to design the experiments. A three-factor and five-level CCD-based RSM was constructed to understand the effects of each process parameter and their interactions on the plasma-assisted ethanol steam reforming process and to predict the optimum process conditions. The plasma-assisted ESR was performed at room temperature and atmospheric pressure. The design of experiments and correlated analysis were performed using the Design Expert software (trial version). Discharge power (X_1), total flow rate (X_2), and EtOH/H_2O molar ratio (X_3) were selected as the three independent variables. EtOH conversion (Y_1), H_2 yield

(Y_2), H_2 selectivity (Y_3), and specific energy requirement (SER) for H_2 production (Y_4) were considered as response factors. Each process parameter has five levels of -1.68, -1, 0, +1, and +1.68 according to (7) [55],

$$x_i = \frac{X_i - X_0}{\Delta X_i} \quad (7)$$

where x_i and X_i are the coded and actual values of the i[th] parameter, respectively. X_0 is the value of the i[th] parameter at the center point within the tested range and ΔX_i is the step size. The coded and actual levels of the process parameters are shown in Table 1. The experimental design matrix for the EtOH steam reforming process is listed in Table 2, a five-level CCD model with 20 experimental sets was designed to optimize the independent process parameters.

Table 1 Independent variables with coded and actual values in CCD

Independent variables	Unit	Coded factors	-1.68	-1	0	1	1.68
Discharge power (X_1)	W	x_1	38	45	55	65	72
Total flow rate (X_2)	ml/min	x_2	26	40	60	80	94
EtOH/H_2O molar ratio (X_3)	-	x_3	0.33	0.6	1	1.4	1.67

In a typical CCD design, a polynomial second-order regression model was used to represent the relationship between the independent variables and output responses. This regression model could be defined as Eq. (8)

$$Y = \beta_0 + \sum_{i=1}^{3} \beta_i x_i + \sum_{i=1}^{3} \beta_{ii} x_{ii}^2 + \sum_{i=1}^{2} \sum_{j=i+1}^{3} \beta_{ij} x_i x_j \quad (8),$$

where Y and x_i are the response and coded value of the independent variables, respectively. β_i, β_{ii}, β_{ij}, and β_0 represented the linear, quadratic, interactions, and constant coefficients, respectively.

Analysis of Variance (ANOVA) was used to evaluate the significance and appropriateness of regression models. The significance of the models was measured by the F-distribution (F-value), P-value, and coefficient of determination (R^2) [56]. The F-value was computed by dividing the mean of square regression (MS_{SSR}) by the mean of square residual (MS_{SSE}). MS_{SSR} and MS_{SSE}

were obtained from the sum of squares (SSR) and the sum of residual (SSE) that were divided by the degree of freedom [48]. ANOVA for Quadratic model results for EtOH conversion, H_2 yield, H_2 selectivity, and specific energy requirement (SER) for H_2 production are shown in Supplementary material Tables S1 through S4, respectively. Multiple response surface analysis and contour plots were used to estimate the interaction between each parameter.

3. Results and Discussion

3.1 Regression models

As designed using RSM, the optimum experiments for DBD plasma-assisted ethanol steam reforming were carried out. Following the design, 20 sets of experiments were performed, and the experimental data is presented in Table 2. Six replicated experimental runs (No. 4, 6, 8, 11, 12, and 19) were employed to estimate the method error. To ensure the adequacy of the suggested model, each experiment was repeated three times with an average taken.

Table 2 Experimental design matrix and results of the EtOH steam reforming.

Trial	Independent variables			Response			
	Discharge power (W)	Total flow rate (ml/min)	EtOH /H_2O	EtOH conversion (%)	Y_{H2} (%)	Y_{CO} (%)	SER (kJ/mol)
1	65	80	1.4	31.36	14.29	45.58	8.71
2	45	40	1.4	29.53	13.04	44.17	13.20
3	38	60	1	22.88	9.19	40.18	12.37
4	55	60	1	33.20	13.61	41.01	12.02
5	45	40	0.6	41.19	18.02	43.75	14.87
6	55	60	1	33.26	15.30	46.00	10.70
7	65	40	1.4	24.48	10.69	43.75	23.26
8	55	60	1	33.71	15.18	45.03	10.79
9	65	80	0.6	36.07	19.95	55.31	9.70

10	55	60	0.33	49.58	22.91	46.23	14.40
11	55	60	1	30.19	13.07	43.29	12.53
12	55	60	1	32.90	14.89	45.25	11.00
13	55	26	1	41.76	19.20	45.98	19.41
14	45	80	1.4	19.00	8.01	42.19	10.76
15	72	60	1	34.13	18.11	53.08	11.81
16	65	40	0.6	49.15	24.87	50.60	15.57
17	45	80	0.6	25.64	9.68	37.76	13.83
18	55	94	1	26.93	12.13	45.06	8.64
19	55	60	1	31.31	13.70	43.75	11.95
20	55	60	1.67	22.76	10.10	44.40	13.00

A lack of fit tests and the model diagnosis were carried out. The lack of fit test is used to determine whether or not the regression model fits the dataset properly [57]. A significant lack of fit indicates poor model fitting and could be caused by incorrect variable selection, experimental design, or the omission of some important terms. The ANOVA details, including the lack of fit tests, were presented in Tables S1-S4. The results indicated that the P values of the lack of fit tests were all greater than 0.05 (significance level) for the four selected responses, indicating that there was no significant lack of fit for all of the fitting. Model diagnosis is used to evaluate model assumptions and identify observations that have a significant and unreasonable impact on the analysis. Figures S1-S4 show the Normal Plot of Residuals, Residuals vs. Predicted plot, and Cook's Distance plot for four responses to see if there was any serious violation of the normality, constant variance, and independence assumptions via residuals. In a Normal Plot of Residuals, the data points are close enough to a straight line to indicate that there is no violation of normality. There are no big residuals and no pattern in the residuals in the Residuals vs. Predicted plot, indicating no violation of the linearity and homoscedasticity assumptions. In terms of Cook's Distance plots, only three

of the observations for which Cook's distance is near to 1 demonstrate that there is no breach of data independence.

The fitting of experimental data produced the quadratic regression equations (Eqs. 9-12) to interpret the relationships between process parameters and responses.

Y_1(EtOH conversion, %) (9)

$$= 52.33522 + 1.68452X_1 - 1.42352X_2 - 35.38079X_3 + 0.012428X_1X_2 - 0.346162X_1X_3 + 0.390141X_2X_3 - 0.015975X_1^2 + 0.001169X_2^2 + 7.00044X_3^2$$

Y_2(H_2 yield, %) (10)

$$= 25.15039 + 0.594597X_1 - 0.809225X_2 - 5.71119X_3 + 0.007528X_1X_2 - 0.412215X_1X_3 + 0.184782X_2X_3 - 0.003364X_1^2 + 0.000943X_2^2 + 4.24554X_3^2$$

Y_3(H_2 selectivity, %) (11)

$$= 51.60672 - 0.390208X_1 - 0.647932X_2 + 28.89008X_3 + 0.009062X_1X_2 - 0.669673X_1X_3 + 0.017767X_2X_3 + 0.007958X_1^2 + 0.001007X_2^2 + 2.07819X_3^2$$

Y_4(SER, kJ/mol) (12)

$$= 17.20144 - 0.005855X_1 + 0.296070X_2 - 21.03040X_3 - 0.010590X_1X_2 + 0.357520X_1X_3 - 0.157711X_2X_3 + 0.002820X_1^2 + 0.002419X_2^2 + 5.37815X_3^2$$

Positive and negative coefficients in Eqs. 9-12 describe the parameters' favorable and unfavorable effects on the responses, respectively [49]. The ANOVA was used to assess the statistical significance and suitability of the regression models, each variable, and their interactions, utilizing F-value, P-value, and R^2 as critical indications. The model or variable had a higher F-value (tabulated with a 95 percent confidence level) and a lower P-value (<0.05), indicating that it was significant. The models for all four responses, as shown in Table 3, are statistically significant in fitting the experimental data with F-values at a P-value <0.05. Furthermore, sufficient precision assesses the signal-to-noise ratio. For EtOH conversion, H_2 yield, H_2 selectivity, and SER, the appropriate precision values are 17.22, 23.17, 14.07, and 16.16, respectively. All of the appropriate precisions were larger than 4, suggesting that the signals were suitable and that the models could be utilized to traverse the design.

The P-plot and coefficient of determination (R^2) were shown in Figure 2, which compared the experimental results and predicted values using regression models for all the responses. The R^2 for each model is greater than 0.9, which suggested that the experimental data agree with the predicted values calculated by the regression models and further confirmed the good adequacy of the regression models.

Table 3 Summary of Analysis of Variance (ANOVA) for the models

Responses	F-value	P-value	Adequate precision	Sum of squares (SS)			Model terms with P-value <0.05
				Total	Residual	Model	
Y_1 (EtOH conversion, %)	24.77	<0.0001	17.22	1277.51	54.85	1222.7	X_1, X_2, X_3, X_1X_2, X_2X_3, X_1^2
Y_2 (H_2 yield, %)	43.53	<0.0001	23.17	393.59	9.8	383.79	X_1, X_2, X_3, X_1X_2, X_1X_3, X_2X_3, X_3^2
Y_3 (H_2 selectivity, %)	12.13	0.0003	14.07	314.7	26.4	288.3	X_1, X_3, X_1X_2, X_1X_3
Y_4 (SER, kJ/mol)	18.11	<0.0001	16.16	230.59	13.33	217.26	X_2, X_1X_2, X_1X_3, X_2X_3, X_2^2, X_3^2

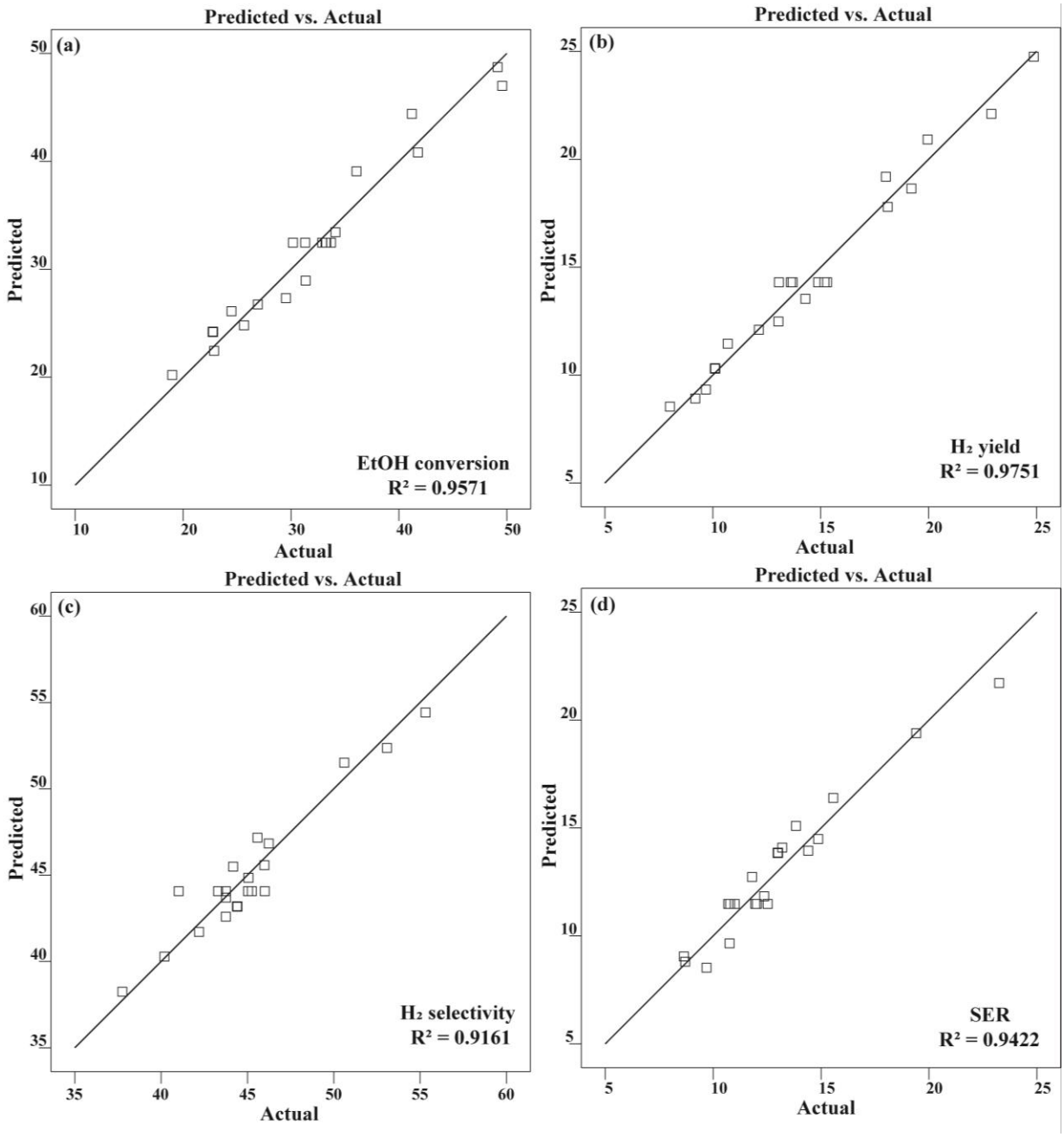

Figure 2 The comparison between predicted and experimental values for (a) EtOH conversion, (b) H_2 yield, (c) H_2 selectivity, and (d) SER for H_2 production.

3.2 Effect of operation parameters on the EtOH conversion

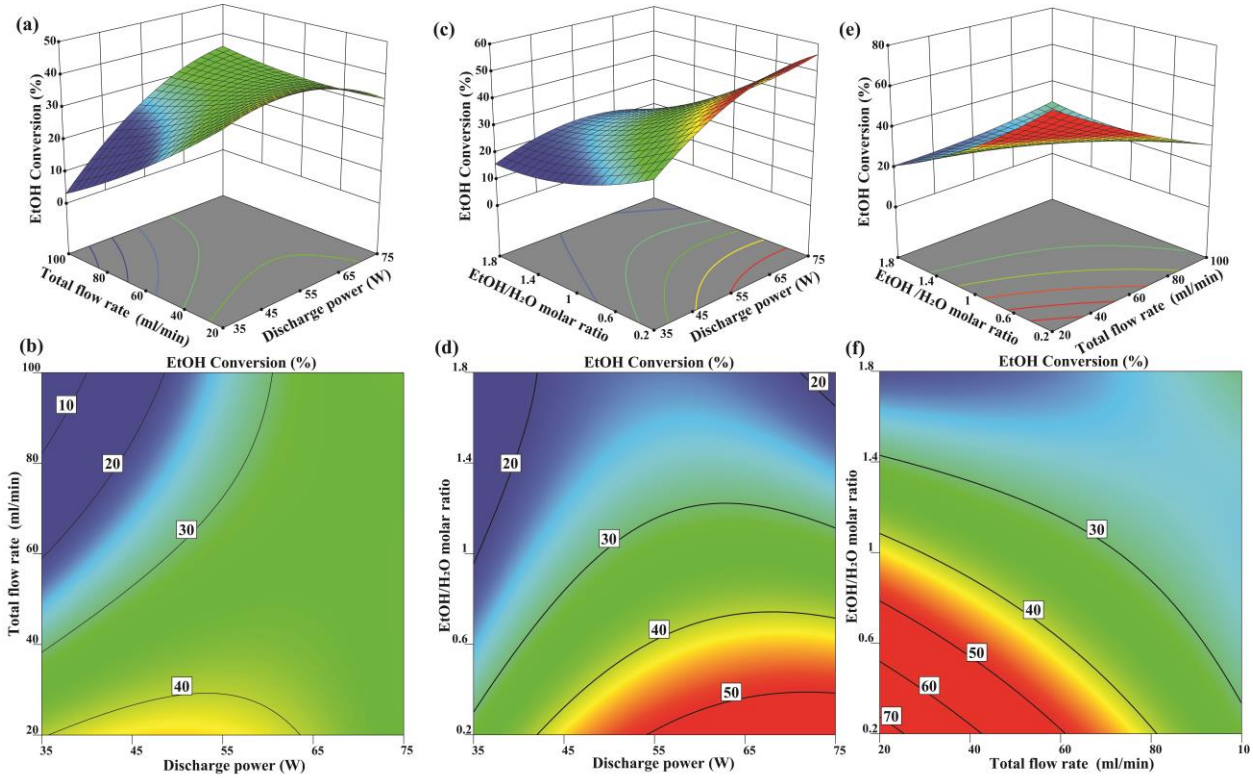

Figure 3 The 3D response surface plots and contour plots of parameter interactions on EtOH conversion: (a-b) the interaction between discharge power and total flow rate at EtOH/H_2O molar ratio of 1.0, (c-d) interaction between EtOH/H_2O molar ratio and discharge power at a total flow rate of 60 ml/min, and (e-f) the interaction between EtOH/H_2O molar ratio and total flow rate at discharge power of 55 W.

The P-value could be used to determine the importance of each item in the regression model for all responses (individual process parameter or interaction of any two parameters). The associated item is regarded as significant in affecting the plasma process if the P-value is less than 0.05. The ANOVA findings showed that the terms X_1, X_2, X_3, X_1X_2, X_2X_3, and X_1^2 were significant factors in the EtOH conversion regression model since their P-values were less than 0.05, as shown in Table 3. The F-value of each significant factor determined its relative importance. The EtOH/H_2O molar ratio (X_3) is considered to have the most significant effect on the EtOH conversion, as it has the largest F-value among all terms in the model.

The interaction between process parameters and their effect on EtOH conversion was plotted as the 3D response surface plots and contour plots, as shown in Figure 3. Figures 3a and 3b demonstrated the interactive effect of discharge power and total flow rate on EtOH conversion.

Figure 3a suggests that the largest EtOH conversion could be observed at the discharge power of around 55 W and the lowest total flow rate of 20 ml/min. Lowering the total flow rate could increase the residence time of reactant gases in the plasma zone and promote the EtOH conversion. At a flow rate of 100 ml/min, EtOH has a residence time of 8.7 s, which is increased to 43.5 s at a flow rate of 20 ml/min. The number of micro discharges and current intensity was dramatically increased in the plasma gap while raising the discharge power by changing the applied voltage. Therefore, more energetic electrons and reaction channels can be provided in the plasma gap for EtOH conversion [47,58]. The power could further be tunned by adjusting the frequency and combined effect of discharge power and total flow rate leading to increased plasma-gas interaction and boosted collision possibility between plasma species and gas molecules [48]. Figure 3b shows a larger gradient of EtOH conversion change on the total flow rate than the discharge power. This indicates that in the combined effect of discharge power and total flow rate, the total flow rate had more impact on EtOH conversion. The overall estimation suggested the interactive effect of discharge power and total flow rate is significant as the P-value of X_1X_2 is less than 0.05.

The interaction of EtOH/H_2O molar ratio and discharge power was considered insignificant in EtOH conversion. The P-value of X_1X_3 is 0.1254, which is greater than the critical value of 0.05. Figures 3c and 3d showed the combined effect of EtOH/H_2O molar ratio and discharge power. At a specific discharge power, EtOH conversion increased along with the reduction of the EtOH/H_2O ratio. More water molecules entered the plasma reaction zone when the EtOH/H_2O ratio was reduced. The electron impact would directly dissociate the water molecules, resulting in reactive species. These reactive species interacted with ethanol molecules, transferring energy, and starting the breakdown process [43,59]. The combined effect of the EtOH/H_2O ratio and total flow rate is regarded as a significant effect because the P-value equals 0.0037, which is less than 0.05. As presented in Figures 3e and 3f, the increasing trend of EtOH conversion with the decrease in EtOH/H_2O ratio is as distinct as the total flow rate, as it shows a similar gradient of EtOH conversion concerning EtOH/H_2O ratio and total flow rate.

3.3 Effect of operation parameters on the production yield of H_2

The ANOVA results, listed in Table 3, suggested that in the regression model of H_2 yield, the terms X_1, X_2, X_3, X_1X_2, X_1X_3, X_2X_3, X_3^2 were considered the significant factors since their P-values of X_1, X_2, X_3, X_1X_2, X_1X_3, X_2X_3, X_3^2 were less than 0.05. The F-value of each significant

factor determined its relative importance. The EtOH/H_2O molar ratio (X_3) is identified as the most influential parameter on the H_2 yield, with the largest F-value of 168.84 among all terms in the model.

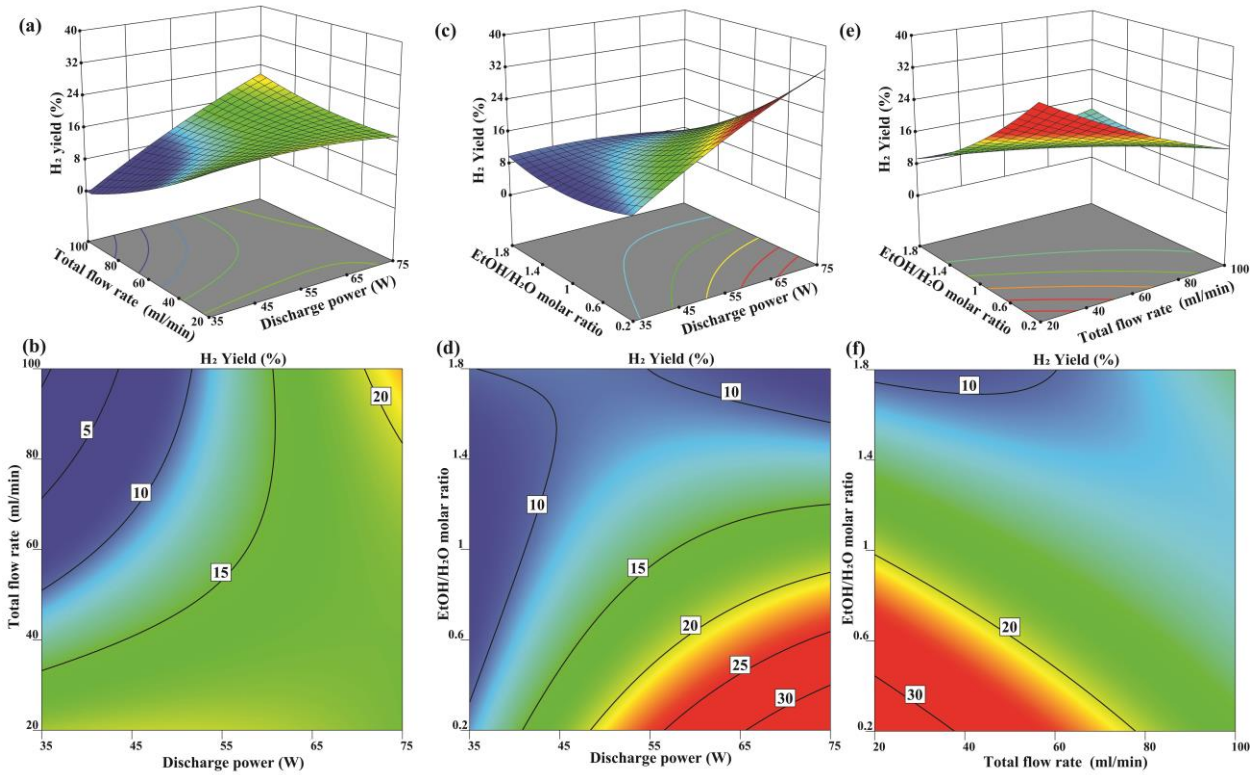

Figure 4 The 3D response surface plots and contour plots of parameter interactions on H_2 yield: (a-b) the interaction between discharge power and total flow rate at EtOH/H_2O molar ratio of 1.0, (c-d) interaction between EtOH/H_2O molar ratio and discharge power at a total flow rate of 60 ml/min, and (e-f) the interaction between EtOH/H_2O molar ratio and total flow rate at discharge power of 55 W.

The interaction between process parameters was evaluated by analyzing the P-values, and their effect on H_2 yield was plotted as the 3D response surface plots and contour plots, as shown in Figure 4. Figures 4a and 4b presented the combined effect of total flow rate and discharge power on the H_2 yield. Increasing the discharge power and reducing the total flow rate simultaneously improved the H_2 yield. At a specific flow rate of 100 ml/min, a larger gradient of H_2 yield changes in the total flow rate than the discharge power. This suggests that the total flow rate had a greater impact on H_2 yield than discharge power did when the two factors were considered as a combined effect. These also indicated that the interaction between total flow rate and discharge power significantly impacted the H_2 yield, which could be confirmed by the P-value of 0.0016. At a low

EtOH/H_2O ratio (0.2-0.6), as shown in Figures 4c-4d, the H_2 yield is more sensitive to the change in discharge power and gradually increases along with the increase of the discharge power. This could be attributed to more energetic electrons, and reaction channels can be provided in the plasma gap, and it is more critical to the H_2 yield compared to the importance of the EtOH/H_2O ratio in the combined effect. In Figures 4e and 4f, the interaction between EtOH/H_2O ratio and the total flow rate is significant, while EtOH/H_2O ratio is dominant. The largest H_2 yield was obtained at the total flow rate of 20 ml/min and an EtOH/H_2O ratio of 0.2. At a small EtOH/H_2O ratio, more water molecules are introduced to the plasma zone. The hydroxyl radical transfers energy and promote ethanol decomposition to generate more H_2 product [42,53]. The free radicals concentration and water gas shift (WSG) reaction, which favors the H_2 equilibrium with additional water added, could also lead to higher H_2 yield.

3.4 Effect of operation parameters on the H_2 selectivity

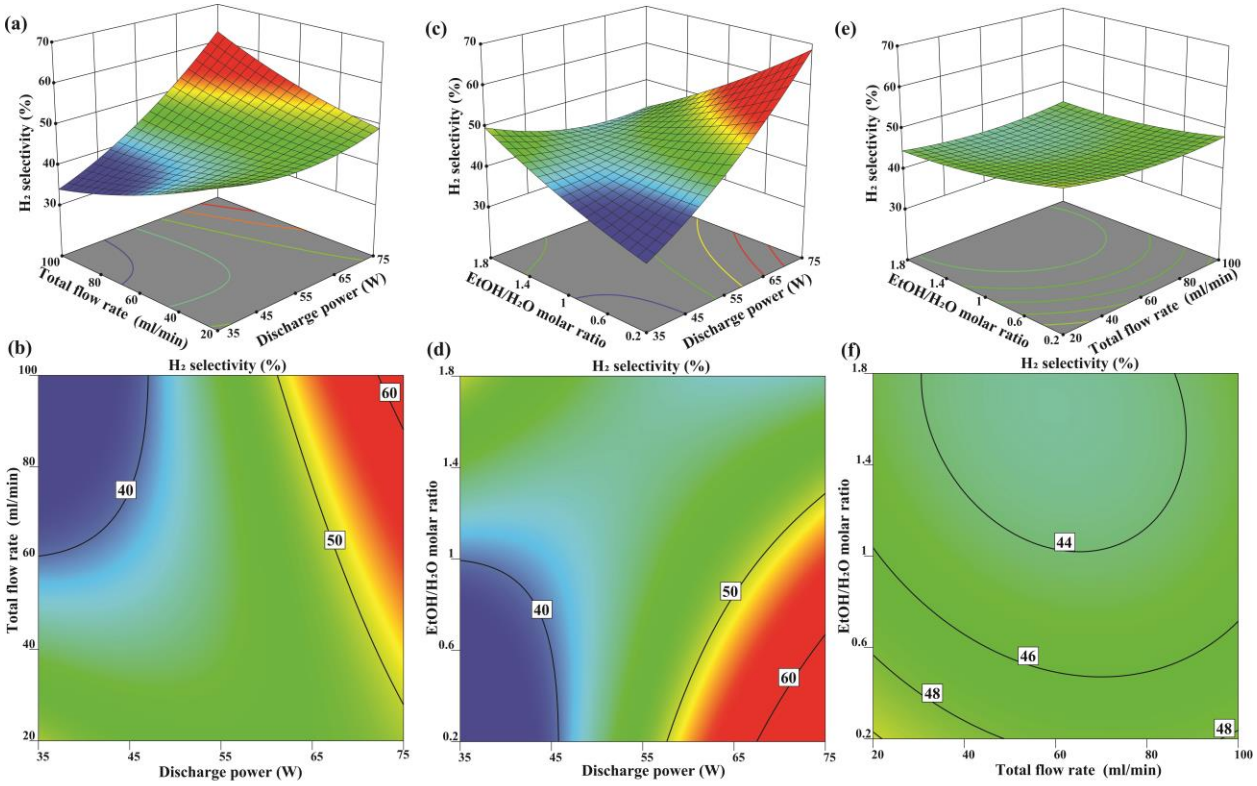

Figure 5 The 3D response surface plots and contour plots of parameter interactions on H_2 selectivity: (a-b) the interaction between discharge power and total flow rate at EtOH/H_2O molar ratio of 1.0, (c-d) interaction between EtOH/H_2O molar ratio and discharge power at a total flow rate of 60 ml/min, and (e-f) the interaction between EtOH/H_2O molar ratio and total flow rate at discharge power of 55 W.

The combined effect of process parameters on H_2 selectivity was plotted as the 3D response surface plots and contour plots, as shown in Figure 5. The ANOVA results in Table 3 suggested that in the regression model of H_2 selectivity, the terms X_1, X_3, X_1X_2, and X_1X_3 were considered the significant factors since the P-values were less than 0.05. Among all these terms, the discharge power (X_1) is identified as the most influential parameter of the H_2 selectivity, with the largest F-value of 66.77 among all terms in the model.

The interaction between total flow rate and discharge power on the H_2 selectivity was presented in Figures 5a and 5b. At a total flow rate of 100 ml/min, the H_2 selectivity is more sensitive to the discharge power, while the H_2 selectivity did not present a massive change in the low flow rate range. The combined effect was significant on H_2 selectivity as its P-value is less than 0.05, though discharge power showed more impact than the total flow rate. Similarly, as shown in Figures 5c and 5d, the cross-impact of EtOH/H_2O molar ratio and discharge power is also significant. At a small EtOH/H_2O ratio, H_2 selectivity gradually increased concerning the discharge power. Figures 5e and 5f presented an approximately parallel distribution of the H_2 selectivity increment along with EtOH/H_2O molar ratio, suggesting that the combined impact of EtOH/H_2O molar ratio and total flow rate is insignificantly detrimental to H_2 selectivity. The reduction in EtOH/H_2O molar ratio plays a critical role in the H_2 selectivity, while H_2 selectivity is less sensitive to the change in the total flow rate. This could also be confirmed by its P-value greater than 0.05.

3.5 Effect of operation parameters on the specific energy requirement (SER) for H_2 production

The specific energy requirement (SER) of H_2 with the unit of kJ/mol was calculated to assess the energy consumption of producing the unit amount of H_2. The combined effect of process parameters on the specific energy requirement (SER) for H_2 production was plotted as the 3D response surface plots and contour plots, as shown in Figure 6. The ANOVA results in Table 3 suggested that in the regression model of SER, the terms X_2, X_1X_2, X_1X_3, X_2X_3, X_2^2, and X_3^2, were considered the significant factors since the P-values were less than 0.05. Regarding the effect of each parameter, the total flow rate (X_2) is identified as the most influential parameter on the SER for H_2 production, with the largest F-value among all terms in the model. The discharge power and total flow rate are more critical than the EtOH/H_2O molar ratio to the SER for H_2.

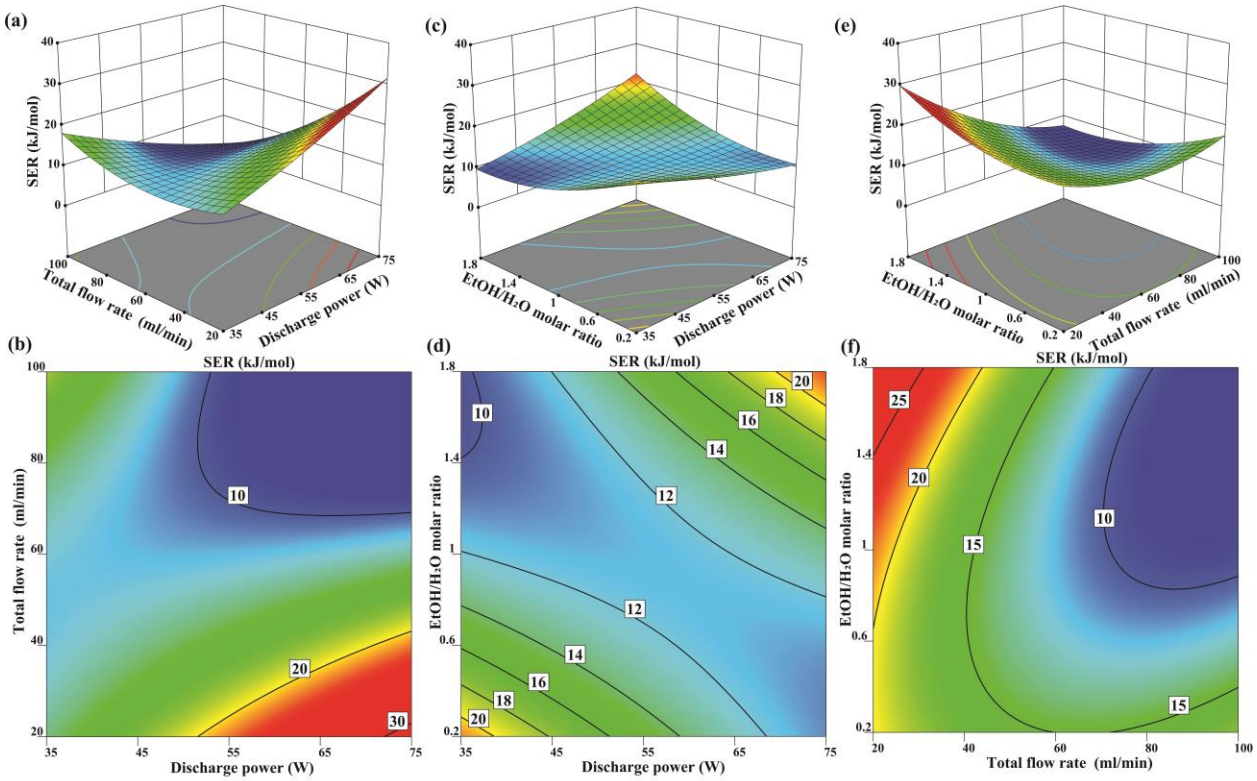

Figure 6 The 3D response surface plots and contour plots of parameter interactions on the specific energy requirement (SER) for H_2 production: (a-b) the interaction between discharge power and total flow rate at EtOH/H_2O molar ratio of 1.0, (c-d) interaction between EtOH/H_2O molar ratio and discharge power at a total flow rate of 60 ml/min, and (e-f) the interaction between EtOH/H_2O molar ratio and total flow rate at discharge power of 55 W.

Figures 6a and 6b demonstrated the interactive effect of discharge power and total flow rate on SER for H_2. The results suggested that the largest SER could be observed at the largest discharge power of 75 W and the lowest total flow rate of 20 ml/min. Reducing the total flow rate and increasing the discharge power increase the residence time and cause more energy costs. Figures 6c and 6d showed that either the combined largest discharge power and largest EtOH/H_2O ratio or the combined least discharge power and least EtOH/H_2O ratio resulted in a large SER. Therefore, the interaction is critical to the SER, and a balance between these two parameters needs to be addressed to maintain a relatively low SER for H_2 production. The combined effect of the EtOH/H_2O ratio and total flow rate is regarded as a significant effect because the P-value equals 0.0114, which is less than 0.05. As presented in Figures 6e and 6f, at the EtOH/H_2O ratio of 1.8, a larger gradient of SER for H_2 concerning total flow rate, suggesting that the total flow rate is more critical than the EtOH/H_2O ratio. Additionally, at the total flow rate of 20 ml/min, the SER

increased markedly, confirming the impact of the EtOH/H_2O ratio and suggesting the significant interaction between the total flow rate and EtOH/H_2O ratio.

3.6 Process optimization and validation

The optimal levels of each variable within the design space in the DBD plasma ESR reaction process were estimated regarding the demand for a high EtOH conversion and high H_2 yield. The optimum conditions for our DBD-plasma reactor include a discharge power of 55.9 W, a total flow rate of 26.7 ml/min, and an EtOH/H_2O molar ratio equal to 0.34. Condersing our reactor dimensions, the optimized conditions would be equal to an specific energy input (SEI) of 32.0 eV/EtOH molecule, a gas hourly space velocity (GHSV) of 101 h^{-1}, and an EtOH/H_2O molar ratio of 0.34. The predicted EtOH conversion is 63.9 %, 31.7 % H_2 yield, and an H_2 selectivity of 49.2 %. The SER for H_2 production in this optimized model is 18.4 kJ/mol. Following the optimum conditions, the validation test was carried out and resulted in an EtOH conversion of 65.5 %, along with H_2 yield and H_2 selectivity of 33.7 % and 51.5 %, respectively. The experimental value of SER for H_2 is 21.81 kJ/mol. Differences between the predicted and experimental values for EtOH conversion, H_2 yield, and H_2 selectivity were in the range of ±5 %, which validated the feasibility of the optimization process.

4. Conclusions

In the present work, the effects of three process parameters on the DBD-plasma ESR for H_2 production were investigated via RSM. Regression models were generated to represent the correlation among all process parameters (discharge power, total flow rate, and EtOH/H_2O molar ratio) with the catalytic performance. Lack of fits and model diagnostics confirmed the validation of the regression models and there is no violation of the observations against the regression assumptions. ANOVA helped to evaluate the significance and adequacy of the regression models. 3D response surface plots and contour plots interpreted the interactive effects of each process parameter. P-plot and coefficient of determination showed that R^2 is greater than 0.9 for all four regression models and suggested good adequacy of the regression models. ANOVA results demonstrated that the EtOH/H_2O molar ratio is considered to have the most significant effect on the EtOH conversion and H_2 yield. The discharge power is the most critical to H_2 selectivity, while the total flow rate is the most significant parameter affecting SER for H_2 production. Interaction between discharge power and total flow rate, discharge power and EtOH/H_2O molar ratio, total

flow rate and EtOH/H_2O molar ratio, all presented significant effects on H_2 yield and the specific energy requirement (SER) for H_2 production. H_2 selectivity was significantly affected by the interactive effect of discharge power and total flow rate, discharge power and EtOH/H_2O molar ratio. Process optimization provided the optimal process conditions, followed by a validation test that was performed and verified the feasibility of the optimization process.

Author contributions

Guoqiang Cao: Methodology; Data curation; Formal analysis; Writing - original draft. **Yue Xiao**: Data curation; Funding acquisition; Writing - review & editing. **Wei-Min Huang:** Methodology; Formal analysis. **Chien-Hua Chen**: Funding acquisition; Writing - review & editing. **Jonas Baltrusaitis:** Conceptualization; Funding acquisition; Supervision; Writing - review & editing.

Acknowledgments

This material is based upon work supported by the U.S. Department of Energy, Small Business Innovation Research and Small Business Technology Transfer program under Award Numbers DE-SC0019664 (Program Manager: Dr. Lei Hong) and DE-SC0020924 (Program Manager: Dr. Naomi R. O'Neil). The authors also thank Prof. Ping-Shi Wu (Department of Mathmetics, Lehigh University) for his critical suggestions on methodology and formal analysis.

References

[1] Abdalla AM, Hossain S, Nisfindy OB, Azad AT, Dawood M, Azad AK. Hydrogen production, storage, transportation and key challenges with applications: A review. Energy Convers Manag 2018;165:602–27. https://doi.org/10.1016/j.enconman.2018.03.088.

[2] Sharma YC, Kumar A, Prasad R, Upadhyay SN. Ethanol steam reforming for hydrogen production: Latest and effective catalyst modification strategies to minimize carbonaceous deactivation. Renew Sustain Energy Rev 2017;74:89–103. https://doi.org/10.1016/j.rser.2017.02.049.

[3] Du C, Mo J, Li H. Renewable hydrogen production by alcohols reforming using plasma and plasma-catalytic technologies: Challenges and opportunities. Chem Rev 2015;115:1503–42. https://doi.org/10.1021/cr5003744.

[4] Dodds PE, Staffell I, Hawkes AD, Li F, Grünewald P, McDowall W, et al. Hydrogen and fuel cell technologies for heating: A review. Int J Hydrogen Energy 2015;40:2065–83. https://doi.org/10.1016/j.ijhydene.2014.11.059.

[5] Schlapbach L, Züttel A. Hydrogen-storage materials for mobile applications. Nature 2001;414:353–8. https://doi.org/10.1038/35104634.

[6] Li A, Kan E, Chen S, Du Z, Liu X, Wang T, et al. Enabling High Loading in Single-Atom Catalysts on Bare Substrate with Chemical Scissors by Saturating the Anchoring Sites. Small 2022;18:2200073. https://doi.org/10.1002/smll.202200073.

[7] Li L, Tang D, Song Y, Jiang B, Zhang Q. Hydrogen production from ethanol steam reforming on Ni-Ce/MMT catalysts. Energy 2018;149:937–43. https://doi.org/10.1016/j.energy.2018.02.116.

[8] Abdul Ghani A, Torabi F, Ibrahim H. Autothermal reforming process for efficient hydrogen production from crude glycerol using nickel supported catalyst: Parametric and statistical analyses. Energy 2018;144:129–45. https://doi.org/10.1016/j.energy.2017.11.132.

[9] Zhang P, Wang T, Gong J. Mechanistic Understanding of the Plasmonic Enhancement for

Solar Water Splitting. Adv Mater 2015;27:5328–42. https://doi.org/10.1002/adma.201500888.

[10] Wang B, Liu S, Peng Y, Wang C, Zou J. Heptane dry reforming and coupling with partial oxidation in gliding arc discharge plasma for H2 production. Fuel Process Technol 2021;221:106943. https://doi.org/10.1016/j.fuproc.2021.106943.

[11] Chen W-H, Farooq W, Shahbaz M, Naqvi SR, Ali I, Al-Ansari T, et al. Current status of biohydrogen production from lignocellulosic biomass, technical challenges and commercial potential through pyrolysis process. Energy 2021;226:120433. https://doi.org/10.1016/j.energy.2021.120433.

[12] Zhang X, Su Y, Pei C, Zhao Z-J, Liu R, Gong J. Chemical looping steam reforming of methane over Ce-doped perovskites. Chem Eng Sci 2020;223:115707. https://doi.org/10.1016/j.ces.2020.115707.

[13] Medrano JA, Oliva M, Ruiz J, García L, Arauzo J. Hydrogen from aqueous fraction of biomass pyrolysis liquids by catalytic steam reforming in fluidized bed. Energy 2011;36:2215–24. https://doi.org/10.1016/j.energy.2010.03.059.

[14] López E, Divins NJ, Anzola A, Schbib S, Borio D, Llorca J. Ethanol steam reforming for hydrogen generation over structured catalysts. Int J Hydrogen Energy 2013;38:4418–28. https://doi.org/10.1016/j.ijhydene.2013.01.174.

[15] Fatih Demirbas M, Balat M, Balat H. Biowastes-to-biofuels. Energy Convers Manag 2011;52:1815–28. https://doi.org/10.1016/j.enconman.2010.10.041.

[16] Dan M, Mihet M, Tasnadi-Asztalos Z, Imre-Lucaci A, Katona G, Lazar MD. Hydrogen production by ethanol steam reforming on nickel catalysts: Effect of support modification by CeO2 and La2O3. Fuel 2015;147:260–8. https://doi.org/10.1016/j.fuel.2015.01.050.

[17] Zhang C, Li S, Wu G, Huang Z, Han Z, Wang T, et al. Steam reforming of ethanol over skeletal Ni-based catalysts: A temperature programmed desorption and kinetic study. AIChE J 2014;60:635–44. https://doi.org/10.1002/aic.14264.

[18] Montero C, Remiro A, Benito PL, Bilbao J, Gayubo AG. Optimum operating conditions in ethanol steam reforming over a Ni/La2O3-αAl2O3 catalyst in a fluidized bed reactor.

Fuel Process Technol 2018;169:207–16. https://doi.org/10.1016/j.fuproc.2017.10.003.

[19] Zhang C, Li S, Li M, Wang S, Ma X, Gong J. Enhanced oxygen mobility and reactivity for ethanol steam reforming. AIChE J 2012;58:516–25. https://doi.org/10.1002/aic.12599.

[20] Riotto T, Cao G, Luyben WL, Baltrusaitis J. Atmospheric Pressure DBD Plasma Ammonia Synthesis and Separation Process Design and Environmental Impact Assessment. ACS Sustain Chem Eng 2021;9:13233–44. https://doi.org/10.1021/acssuschemeng.1c04031.

[21] Zhou R, Zhou R, Xian Y, Fang Z, Lu X, Bazaka K, et al. Plasma-enabled catalyst-free conversion of ethanol to hydrogen gas and carbon dots near room temperature. Chem Eng J 2020;382. https://doi.org/10.1016/j.cej.2019.122745.

[22] Pearlman H, Giles M, Chen C-H, Demydovych M, Kiani D, Baltrusaitis J. Plasma-Assisted Dry Methane Reforming for Syngas Production. Spring Tech Meet East States Sect Combust Inst 2018;2:0–1.

[23] Liu S, Mei D, Wang L, Tu X. Steam reforming of toluene as biomass tar model compound in a gliding arc discharge reactor. Chem Eng J 2017;307:793–802. https://doi.org/10.1016/j.cej.2016.08.005.

[24] Mei D, Tu X. Conversion of CO2 in a cylindrical dielectric barrier discharge reactor: Effects of plasma processing parameters and reactor design. J CO2 Util 2017;19:68–78. https://doi.org/10.1016/j.jcou.2017.02.015.

[25] Cao G, Handler RM, Luyben WL, Xiao Y, Chen C, Baltrusaitis J. CO 2 conversion to syngas via electrification of endothermal reactors : Process design and environmental impact analysis. Energy Convers Manag 2022;265:115763. https://doi.org/10.1016/j.enconman.2022.115763.

[26] Rouwenhorst KHR, Mani S, Lefferts L. Improving the Energy Yield of Plasma-Based Ammonia Synthesis with In Situ Adsorption. ACS Sustain Chem Eng 2022;10:1994–2000. https://doi.org/10.1021/acssuschemeng.1c08467.

[27] Song L, Liang T, Liu C, Li X. Experimental investigation of hydrogen production by CH4–CO2 reforming using rotating gliding arc discharge plasma. Int J Hydrogen Energy

2019;44:29450–9. https://doi.org/10.1016/j.ijhydene.2019.05.245.

[28] Du C, Huang D, Mo J, Ma D, Wang Q, Mo Z, et al. Renewable hydrogen from ethanol by a miniaturized nonthermal arc plasma-catalytic reforming system. Int J Hydrogen Energy 2014;39:9057–69. https://doi.org/10.1016/j.ijhydene.2014.04.041.

[29] Kai Z, Feilong S, Di J, Shida X, Jiulun S, Shengfang H. Experimental investigation on the cracking of pre-combustion cracking gas with gliding arc discharge plasma. Int J Hydrogen Energy 2021;46:9019–29. https://doi.org/10.1016/j.ijhydene.2020.12.226.

[30] Jiménez M, Rincón R, Marinas A, Calzada MD. Hydrogen production from ethanol decomposition by a microwave plasma: Influence of the plasma gas flow. Int J Hydrogen Energy 2013;38:8708–19. https://doi.org/10.1016/j.ijhydene.2013.05.004.

[31] Rincón R, Muñoz J, Morales-Calero FJ, Orejas J, Calzada MD. Assessment of two atmospheric-pressure microwave plasma sources for H2 production from ethanol decomposition. Appl Energy 2021;294:116948. https://doi.org/10.1016/j.apenergy.2021.116948.

[32] Liu J-L, Zhu TH, Sun B. Understanding the chemical kinetics for plasma in liquid: Reaction mechanism of ethanol reforming in microwave discharge. Int J Hydrogen Energy 2022;47:12841–54. https://doi.org/10.1016/j.ijhydene.2022.02.041.

[33] Bundaleska N, Tsyganov D, Tatarova E, Dias FM, Ferreira CM. Steam reforming of ethanol into hydrogen-rich gas using microwave Ar/water “tornado” – Type plasma. Int J Hydrogen Energy 2014;39:5663–70. https://doi.org/10.1016/j.ijhydene.2014.01.194.

[34] Tsyganov D, Bundaleska N, Tatarova E, Ferreira CM. Ethanol reforming into hydrogen-rich gas applying microwave ‘tornado’-type plasma. Int J Hydrogen Energy 2013;38:14512–30. https://doi.org/10.1016/j.ijhydene.2013.08.127.

[35] Tu X, Whitehead JC. Plasma-catalytic dry reforming of methane in an atmospheric dielectric barrier discharge: Understanding the synergistic effect at low temperature. Appl Catal B Environ 2012;125:439–48. https://doi.org/10.1016/j.apcatb.2012.06.006.

[36] King B, Patel D, Zhu Chen J, Drapanauskaite D, Handler R, Nozaki T, et al. Comprehensive process and environmental impact analysis of integrated DBD plasma

steam methane reforming. Fuel 2021;304:121328. https://doi.org/10.1016/j.fuel.2021.121328.

[37] Wu Y-W, Chung W-C, Chang M-B. Modification of Ni/γ-Al2O3 catalyst with plasma for steam reforming of ethanol to generate hydrogen. Int J Hydrogen Energy 2015;40:8071–80. https://doi.org/10.1016/j.ijhydene.2015.04.053.

[38] Hu YP, Li G, Yang Y, Gao X, Lu Z. Hydrogen generation from hydro-ethanol reforming by DBD-plasma. Int J Hydrogen Energy 2012;37:1044–7. https://doi.org/10.1016/j.ijhydene.2011.02.147.

[39] Murashkina TL, Syrtanov MS, Laptev RS, Lider AM. Cyclic stability of the C36-type TiCr2 Laves phase synthesized in the abnormal glow discharge plasma under hydrogenation. Int J Hydrogen Energy 2019;44:6709–19. https://doi.org/10.1016/j.ijhydene.2019.01.150.

[40] Li D, Li X, Bai M, Tao X, Shang S, Dai X, et al. CO2 reforming of CH4 by atmospheric pressure glow discharge plasma: A high conversion ability. Int J Hydrogen Energy 2009;34:308–13. https://doi.org/10.1016/j.ijhydene.2008.10.053.

[41] Doroodmand MM, Darabpour M. Image processing of non-thermal glow discharge plasma during gas ionization process as a novel hydrogen detection system at parts per billion levels. Int J Hydrogen Energy 2014;39:3564–71. https://doi.org/10.1016/j.ijhydene.2013.12.101.

[42] Wang B, Lü Y, Zhang X, Hu S. Hydrogen generation from steam reforming of ethanol in dielectric barrier discharge. J Nat Gas Chem 2011;20:151–4. https://doi.org/10.1016/S1003-9953(10)60160-0.

[43] Du C, Mo J, Tang J, Huang D, Mo Z, Wang Q, et al. Plasma reforming of bio-ethanol for hydrogen rich gas production. Appl Energy 2014;133:70–9. https://doi.org/10.1016/j.apenergy.2014.07.088.

[44] MacQueen B, Jayarathna R, Lauterbach J. Knowledge extraction in catalysis utilizing design of experiments and machine learning. Curr Opin Chem Eng 2022;36:100781. https://doi.org/10.1016/j.coche.2021.100781.

[45] Raheem AT, Aziz ARA, Zulkifli SA, Baharom MB, Rahem AT, Ayandotun WB. Optimisation of operating parameters on the performance characteristics of a free piston engine linear generator fuelled by CNG–H2 blends using the response surface methodology (RSM). Int J Hydrogen Energy 2022;47:1996–2016. https://doi.org/10.1016/j.ijhydene.2021.10.125.

[46] Fatah NAA, Jalil AA, Salleh NFM, Hamid MYS, Hassan ZH, Nawawi MGM. Elucidation of cobalt disturbance on Ni/Al2O3 in dissociating hydrogen towards improved CO2 methanation and optimization by response surface methodology (RSM). Int J Hydrogen Energy 2020;45:18562–73. https://doi.org/10.1016/j.ijhydene.2019.04.119.

[47] Mei DH, Liu SY, Tu X. CO2 reforming with methane for syngas production using a dielectric barrier discharge plasma coupled with Ni/γ-Al2O3 catalysts: Process optimization through response surface methodology. J CO2 Util 2017;21:314–26. https://doi.org/10.1016/j.jcou.2017.06.020.

[48] Khoja AH, Tahir M, Saidina Amin NA. Process optimization of DBD plasma dry reforming of methane over Ni/La2O3MgAl2O4 using multiple response surface methodology. Int J Hydrogen Energy 2019;44:11774–87. https://doi.org/10.1016/j.ijhydene.2019.03.059.

[49] Jiang N, Zhao Y, Qiu C, Shang K, Lu N, Li J, et al. Enhanced catalytic performance of CoOx-CeO2 for synergetic degradation of toluene in multistage sliding plasma system through response surface methodology (RSM). Appl Catal B Environ 2019;259:118061. https://doi.org/10.1016/j.apcatb.2019.118061.

[50] Liu J, Zhu X, Zhou C, Du J, Gan Y, Chen G, et al. mPlasma-assisted ammonia synthesis in a packed-bed DBD reactor over M/BaTiO3 (M = Fe, Co and Ni): Process optimization towards cost-effective ammonia synthesis using RSM. Vacuum 2022:111205. https://doi.org/10.1016/j.vacuum.2022.111205.

[51] Barboun PM, Daemen LL, Waitt C, Wu Z, Schneider WF, Hicks JC. Inelastic Neutron Scattering Observation of Plasma-Promoted Nitrogen Reduction Intermediates on Ni/γ-Al2O3. ACS Energy Lett 2021;6:2048–53. https://doi.org/10.1021/acsenergylett.1c00643.

[52] Andersen JA, Christensen JM, Østberg M, Bogaerts A, Jensen AD. Plasma-catalytic dry reforming of methane: Screening of catalytic materials in a coaxial packed-bed DBD reactor. Chem Eng J 2020;397:125519. https://doi.org/10.1016/j.cej.2020.125519.

[53] Du C, Li H, Zhang L, Wang J, Huang D, Xiao M, et al. Hydrogen production by steam-oxidative reforming of bio-ethanol assisted by Laval nozzle arc discharge. Int J Hydrogen Energy 2012;37:8318–29. https://doi.org/10.1016/j.ijhydene.2012.02.166.

[54] Du C, Ma D, Wu J, Lin Y, Xiao W, Ruan J, et al. Plasma-catalysis reforming for H2 production from ethanol. Int J Hydrogen Energy 2015;40:15398–410. https://doi.org/10.1016/j.ijhydene.2015.09.096.

[55] Copeland KAF. Applied Linear Statistical Models. vol. 29. 1997. https://doi.org/10.1080/00224065.1997.11979760.

[56] Montgomery DC. Design and Analysis of Experiments Ninth Edition. 2017.

[57] Montgomery DC. Introduction to Linear Regression Analysis Fifth Edition, 2012.

[58] Zhu X, Tu X, Mei D, Zheng C, Zhou J, Gao X, et al. Investigation of hybrid plasma-catalytic removal of acetone over CuO/γ-Al2O3 catalysts using response surface method. Chemosphere 2016;155:9–17. https://doi.org/10.1016/j.chemosphere.2016.03.114.

[59] Tu X, Yu L, Yan JH, Cen KF, Chéron BG. Dynamic and spectroscopic characteristics of atmospheric gliding arc in gas-liquid two-phase flow. Phys Plasmas 2009;16:113506. https://doi.org/10.1063/1.3266420.